Effect of metal-ion doping on the characteristics and photocatalytic activity of TiO_2 nanotubes for the removal of toluene from water

Rongfang Yuan, Beihai Zhou, Duo Hua, Chunhong Shi and Li Ma

ABSTRACT

Toluene is an extensively used reagent that could cause water pollution and endanger human health. In this work, an O_3/UV/ion-doped TiO_2 nanotubes process was investigated to obtain the optimum TiO_2 nanotubes for effective toluene decomposition. Photocatalytic activity is found to be influenced by the doped-ion type by affecting the ionic radius, valence state, and configuration of the dopant. The calcination temperature and doping concentration, which change the weight fractions of the anatase phase (f_A), the Brunauer–Emmett–Teller surface area (S_{BET}), and the energy band gap (E_g) of the catalyst, also affect the photocatalytic activity. When TiO_2 is doped with ions, S_{BET} decreases and E_g becomes narrower. The photocatalytic activities of TiO_2 for toluene removal increase after doping with Ag^+, Al^{3+}, Cu^{2+}, Fe^{3+}, Mn^{2+}, Ni^{2+}, V^{5+}, and Zn^{2+}. Moreover, the 1.0% Fe^{3+}-doped TiO_2 nanotubes calcined at 550 °C have the highest catalytic activity, with a toluene removal efficiency of 70.7%.

Key words | ion-doping, mechanism, TiO_2 nanotubes, toluene, UV photocatalytic ozonation

Rongfang Yuan
Beihai Zhou (corresponding author)
Duo Hua
Chunhong Shi
Department of Environmental Engineering,
School of Civil and Environmental Engineering,
University of Science and Technology Beijing,
No. 30 Xueyuan Road,
Beijing 100083,
China
and
Key Laboratory of Educational Ministry for High Efficiency Mining and Safety in Metal Mines,
University of Science and Technology Beijing,
Beijing 100083,
China
E-mail: *zhoubeihai@sina.com*

Li Ma
PetroChina Huabei Petrochemical Company,
Renqiu,
Hebei 062552,
China

INTRODUCTION

Toluene is extensively used for the preparation of many compounds, such as benzaldehyde, benzyl alcohol, benzoic acid, and chloro derivatives; it is also used as base chemicals to synthesize dyes, pigment inks, explosives, and medicines (Takeuchi *et al.* 2012). These applications cause water pollution and endanger human health.

Several techniques have been developed to treat toluene. One of which is ultraviolet (UV) photocatalytic ozonation that is highly efficient in generating •OH for the degradation of pollutants (Lin & Lin 2007).

Choosing the appropriate photocatalyst is essential for removing toluene, and TiO_2 is a good candidate. TiO_2-photocatalyzed reactions are non-selective oxidation processes in mg/L level, and the use of TiO_2 is effective for inactive substrates (Carp *et al.* 2004). Moreover, the presence of TiO_2 can provide additional nuclei for bubble formation, thereby enhancing the degradation of pollutants (Adewuyi 2001).

Compared with the powder form, TiO_2 nanotubes have a larger specific surface area. This surface area increases the available Brunauer–Emmett–Teller (BET) surface area (S_{BET}) for the separation of electron-hole pairs and subsequently enhances electron transfer, as well as the interpenetration of holes (Pang & Abdullah 2012a). However, the relatively wide band gap of TiO_2 (3.2 eV) limits the efficiency of photocatalytic reactions because of the high recombination rate of photogenerated electrons and holes (Sun *et al.* 2009). Metal ion-doped TiO_2 nanotubes have been studied to solve this problem (Pang & Abdullah 2012b). Nevertheless, to the best of our knowledge, most studies have focused on the photocatalytic degradation of gaseous toluene, and no study has reported on the application of O_3/UV/ion-doped TiO_2 nanotubes for the removal of toluene from water.

In this work, we investigated the effect of metal-ion doping on the photocatalytic activity of TiO_2 nanotubes in removing toluene through the O_3/UV method. Eight types of metal ions were investigated, namely, Ag^+, Al^{3+}, Cu^{2+}, Fe^{3+}, Mn^{2+}, Ni^{2+}, V^{5+}, and Zn^{2+}, and Fe^{3+} elicited optimum results. Characteristic analyses of the TiO_2 nanotubes were implemented to reveal the influencing factors on the photocatalytic activities of the catalysts (Zwilling *et al.* 1999). In addition, control experiments

doi: 10.2166/wst.2014.071

were conducted to investigate the effects of O_3, UV, and UV/Fe^{3+}-doped TiO_2 processes for toluene removal, and the mechanism of the O_3/UV/Fe^{3+}-doped TiO_2 process was discussed.

METHODS

Material

P-25 TiO_2 was provided by the Degussa Corporation (Richfield Park, New Jersey). The powder has an S_{BET} of 50 m^2/g, an average crystallite size of 21 nm, and a crystal structure of 80% anatase and 20% rutile. Toluene, $AgNO_3$, $AlC1_3$, $CuCl_2 \cdot 2H_2O$, $Fe(NO_3)_3 \cdot 9H_2O$, $Mn(NO_3)_2 \cdot 4H_2O$, $NiC1_2$, NH_4VO_3, and $ZnCl_2$ (A.R.) were purchased from the Beijing Chemical Reagent Company.

A photocatalytic reactor (60 mm in diameter and 750 mm long), equipped with a 37 W 254 nm UV lamp, was purchased from Haili Lighting Equipment Company (Beijing) and was used in the experiment.

Preparation of TiO_2 nanotubes

One gram of P-25 TiO_2 was added to a 16 mL of a 10 mol/L NaOH solution in a Teflon vessel. The mixture was stirred for 2 h at room temperature, heated at 110 °C for 24 h in an oven, and cooled to room temperature in air. The as-prepared precipitate was washed with distilled water until the pH was 7, and was subsequently dispersed in a 0.1 mol/L HCl aqueous solution (0.1 mol/L HNO_3 solution for Ag^+-doping). The precipitate was ultrasonicated for 30 min, washed until the pH was 7, and then dried at 60 °C. The nanotubes were prepared by calcining the precipitate at 550 °C for 2 h. In these reactions, NaOH initially disturbed the crystalline structure of P-25 TiO_2. The free octahedra reassembled and linked together, and then the anatase phase grew longitudinally. The lateral growth led to the formation of two-dimensional crystalline sheets. The crystalline sheets rolled up and decreased the total energy, thereby saturating the dangling bonds and reducing the specific area, and resulting in the formation of TiO_2 nanotubes (Wang *et al.* 2004).

The ion-doped TiO_2 nanotubes were prepared based on the above procedure except that metal salts were doped at 1.0% (atomic concentration). The metal salts used as precursors for dopant ions were $AgNO_3$, $AlC1_3$, $CuCl_2 \cdot 2H_2O$, $Fe(NO_3)_3 \cdot 9H_2O$, $Mn(NO_3)_2 \cdot 4H_2O$, $NiC1_2$, NH_4VO_3, and $ZnCl_2$.

Characterization of TiO_2 nanotubes

X-ray diffraction (XRD) patterns were collected by a Rigaku Dmax-RB diffractometer (Tokyo, Japan). The surface elemental composition of TiO_2 was recorded by an X-ray photoelectron spectroscopy (XPS; AXIS ULTRA^{DLD}, Kratos Analytical, UK). Transmission electron microscopy (TEM) images were obtained by a HITACHI HT-7700 electron microscope (Tokyo, Japan). S_{BET} was measured by Quadrasorb SI-MP apparatus (Quantachrome Instruments, USA). Diffuse reflectance spectroscopy (DRS) analyses were performed using a HITACHI U-3010 UV-vis scanning spectrophotometer (Tokyo, Japan).

The weight fractions of the anatase in anatase-rutile mixtures in the samples (f_A) were calculated by Equation (1) (Spurr & Myers 1957) based on the XRD patterns of the catalyst.

$$f_A = \frac{1}{1 + 1.265\frac{I_R}{I_A}} \quad (1)$$

where I_R and I_A are the maximum XRD peak intensity of the rutile phase (110) and the anatase phase (101).

The UV-vis DRS analysis of the catalysts were conducted to obtain the energy band gaps (E_g). TiO_2 nanotubes had an indirect band gap, and relationship plots were used:

$$F(R_\infty)h\gamma = A(h\gamma - E_g)^2 \quad (2)$$

where $F(R_\infty)$ is the Kubelka–Munk (K–M) function, h is the Planck constant, and γ is the frequency. The value of $F(R_\infty)$ can be estimated using the K–M formula:

$$F(R_\infty) = K/S = \frac{(1 - R_\infty)^2}{2R_\infty} \quad (3)$$

where R_∞ is the diffuse reflectance.

Photocatalytic activity tests

Aqueous slurries were prepared by adding 0.15 g of TiO_2-based photocatalyst to 1,500 mL of 2.25 mg/L toluene aqueous solution with a pH of 7. The aqueous slurries were stirred and bubbled with O_3 (1 L/min, 10%) and irradiated with a 254 nm UV lamp. Every 10 min, a 200 mL sample was acquired. The toluene concentrations were analyzed through the solvent extraction-capillary gas chromatography

method (GB/T 5750.12-2006, China), and a GC-FID gas chromatograph (Agilent 7890A, USA) was used. The temperatures of the injector and the FID (flame ionization detector) of GC were 210 and 220 °C, respectively. The temperature program comprised two phases: the temperature was set at 50 °C for 10 min initially, and then ramped upto 80 °C at a rate of 10 °C/min and held for 3 min.

RESULTS AND DISCUSSION

Characterization of photocatalysts

Morphology of the catalysts

The TEM image of 550 °C calcined Fe^{3+}-doped TiO_2 nanotubes (Figure 1(a)) shows that the nanotubes were successfully synthesized. Moreover, other ion-doped nanotubes share a similar morphology. The Fe^{3+}-doped TiO_2 nanotubes have an average diameter of approximately 8 nm with a hollow and open-ended structure.

XRD analysis

XRD patterns and the f_A of the TiO_2 nanotubes are shown in Figure 1(b) and Table 1. Anatase and rutile phases in TiO_2 nanotubes existed. The characteristic peaks of the (101) crystal plane of anatase and the (110) crystal plane of rutile were located at about 25.3° and 27.4°, respectively. Compared with those of undoped TiO_2, the Bragg angles of the (101) peak position of the ion-doped TiO_2 shifted to lower angles, and the anatase peak intensities decreased. These results occurred because the crystallite has numerous crystal planes caused by ion doping; thus, such crystallite cannot be considered as an ideal crystal. Furthermore, the dopant ions substitute Ti^{4+} in the lattice, which resulted in the deformation of the crystal lattice. Therefore, broadening diffraction peak and decreasing peak intensity were observed. Among the dopant ions, only Ag^+ is observed in the XRD patterns in the form of Ag_2O based on the characteristic peak of the (111) crystal plane of Ag_2O at 32.8° and the XPS spectra of Ag 3d; this result is attributed to the difficulty of Ag^+ in entering the TiO_2 lattice (Epifani *et al.* 2000). Other ions are partially dispersed in the bulk of TiO_2 nanotubes (Pang & Abdullah 2012b). The metallic oxides from other doped ions may also be formed on the surface of TiO_2. However, these oxides are not observed in the XRD patterns because their metal sites are below the visibility limit of X-ray analysis (Ravichandran *et al.* 2009).

XPS analysis

XPS analysis was performed to determine the surface composition and the chemical state of the elements in the catalysts. The binding energies of Ag 3d, Al 2p, Cu 2p, Fe 2p, Mn 2p, Ni 2p, V 2p, and Zn 2p (Table 1) for 550 °C calcined catalysts indicate that the doping ions existed as Ag^+, Al^{3+}, Cu^{2+}, Fe^{3+}, Mn^{2+}, Ni^{2+}, V^{5+}, and Zn^{2+} in the lattice. The binding energies from 458.15 to 459.65 eV for the TiO_2 nanotubes correspond to the peaks of Ti 2p3/2, whereas those from 464.05 eV to 464.70 eV correspond to Ti 2p1/2, thereby indicating that Ti existed as Ti^{4+}. The Ti 2p binding energy of the ion-doped TiO_2 nanotubes increased compared with that of the pure TiO_2 because the electrons in the conduction band of the TiO_2 may have transferred to the doped metal ions on the surface of the TiO_2, which resulted in a decrease in the outer electron cloud density of the Ti ions (Li *et al.* 2011). Compared with the binding energies of the Ti 2p for the 550 °C calcined ion-doped TiO_2, the binding energies for the 60 °C calcined ion-doped TiO_2 increased insignificantly. This result indicates the formation of Ti–O–(doping-ion) bonds in the crystal lattice during calcination.

The oxygen groups in the spectra of O 1s (Figure 1(c)) for the 550 °C calcined catalysts are distributed in the form of crystal lattice oxygen (O^{2-}), which is in accordance with the binding energies from 529.9 to 530.9 eV. The peak located at 529.9 eV is assigned to the oxygen bound to Ti^{4+} (TiO_2) (Leinen *et al.* 1996). Moreover, the O 1s binding energy of the ion-doped TiO_2 nanotubes increased, unlike that of the pure TiO_2.

Surface area analysis

The catalytic efficiencies of TiO_2 nanotubes are related to the S_{BET} of the catalyst (Zhang *et al.* 2012). A larger S_{BET} benefits the adsorption of pollutants on the surface of TiO_2 where the pollutants are degraded by O_3, and more areas are supplied for electron-hole pair separation. The S_{BET} of ion-doped TiO_2 nanotubes are smaller than that of undoped TiO_2 nanotubes, particularly for Ag^+-, Mn^{2+}-, and Ni^{2+}-doped TiO_2 nanotubes (Table 1). The S_{BET} decreases when TiO_2 is doped by ions because of the partial pore blockages and framework defects (Pang & Abdullah 2012b). The S_{BET} of the TiO_2 nanotubes is

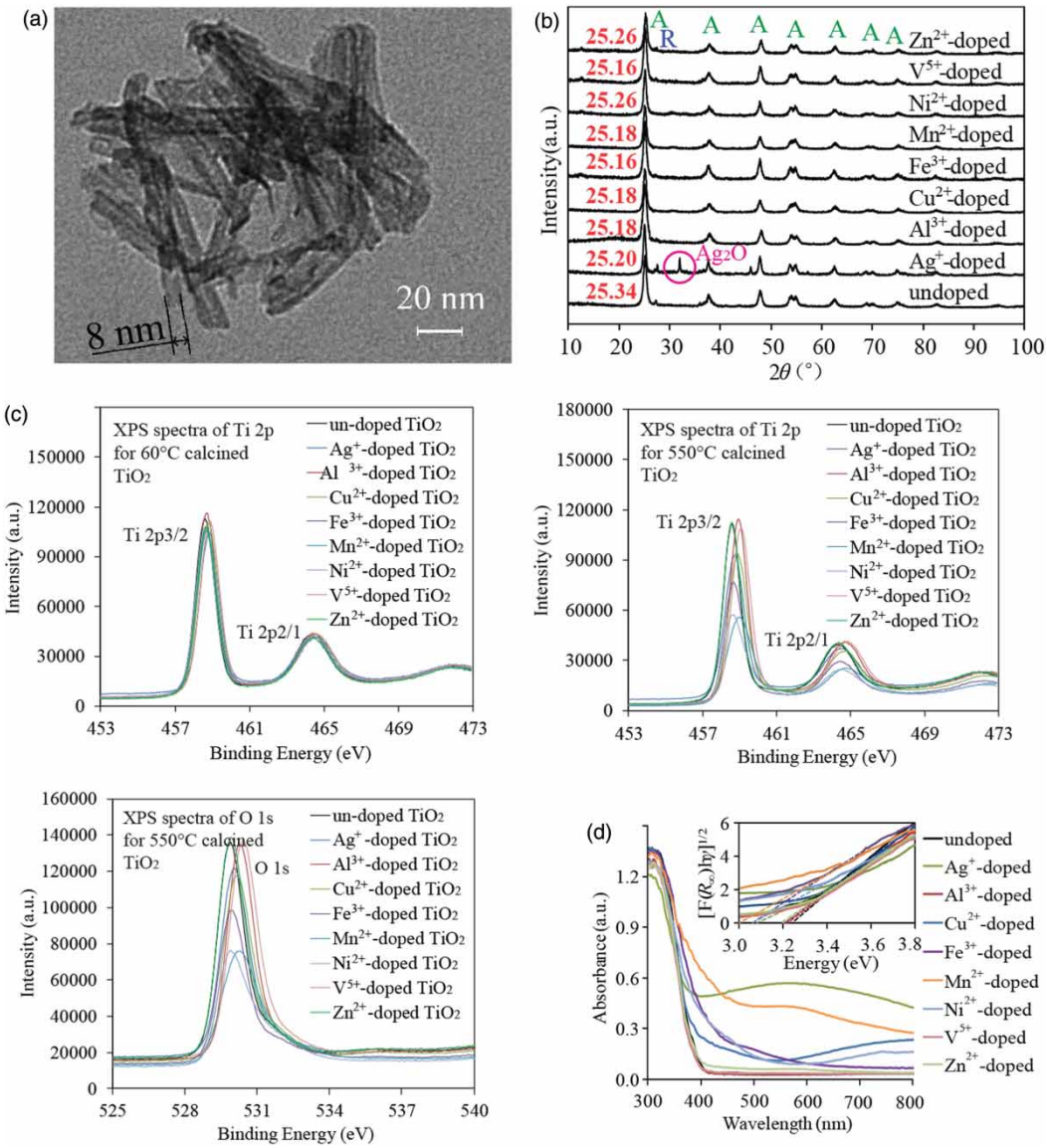

Figure 1 | Characterization of TiO_2 nanotubes. (a) TEM image of Fe^{3+}-doped TiO_2; (b) XRD patterns of the catalysts; 'A' refers to the anatase phase; 'R' refers to the rutile phase; (c) XPS spectra of Ti 2p and O 1s; (d) UV-vis DRS and energy band gap of TiO_2 nanotubes.

significantly larger than that of P-25 TiO_2 because of the inner and outer surfaces of the layered-tubular structure, which is one of the special qualities of the nanotubes (Pang & Abdullah 2012a).

UV-vis DRS analysis

The reflectance spectra of ion-doped TiO_2 slightly shift toward longer wavelength (red shift) as compared with that of the undoped TiO_2, and the E_g of the ion-doped TiO_2 is visibly narrower (Figure 1(d); Table 1). This result revealed that the doped elements involved are indeed incorporated into the lattice of the TiO_2 nanotubes; therefore, doped elements altered the crystal and electronic structures of the lattice of the TiO_2 nanotubes (Yu *et al.* 2009). The reduction in E_g of the TiO_2 nanotubes allows the excitation of the catalyst under lower power of irradiation, and thereby enhances the photocatalytic activity of the catalyst. Moreover, the ion-doped TiO_2 nanotubes display various colours depending on the type of doping-ions: Ag^+-doped nanotubes appear in grayish, Al^{3+}-doped and Zn^{2+}-doped white, Cu^{2+}-doped bluish, Fe^{3+}-doped orange, Mn^{2+}-doped pink, Ni^{5+}-doped greenish, and V^{5+}-doped yellowish. The E_g of the ion-doped TiO_2 is related to the colour

Table 1 | Catalytic properties of the catalysts

Type of catalysts	f_A (%)	Binding energy of doped ions (eV)	E_g (eV)	S_{BET} (m^2/g)
Undoped	83.4	–	3.24	123
Ag^+-doped	84.6	Ag 3d 5/2 (368.3)/3/2 (374.2)	3.12	56
Al^{3+}-doped	86.0	Al 2p (75.7)	3.22	123
Cu^{2+}-doped	91.3	Cu 2p 3/2 (933.2)/1/2 (953.6)	3.21	99
Fe^{3+}-doped	87.5	Fe 2p 3/2 (710.9)/1/2 (726.3)	3.06	118
Mn^{2+}-doped	91.3	Mn 2p 3/2 (642.5)/1/2 (653.9)	3.00	61
Ni^{2+}-doped	88.5	Ni 2p 3/2 (855.5)/1/2 (871.9)	3.06	48
V^{5+}-doped	85.3	V 2p 3/2 (517.4)/1/2 (524.7)	3.20	123
Zn^{2+}-doped	81.5	Zn 2p 3/2 (1021.8)/1/2 (1044.7)	3.19	134

of the catalyst. A darker appearance of the catalyst elicits a narrower E_g.

Photocatalytic activity of the catalysts

Influence of doping ions

Photocatalytic activity tests were conducted to investigate the effects of the dopant types on the catalytic activities of the catalysts (Figures 2(a) and 2(b)). The removal rate of toluene increases when TiO_2 nanotubes are doped by ions because the existing impurity band reduces the recombination of the photoinduced electron-hole; the photoinduced electron-hole can transfer electrons more efficiently to the oxygen adsorbed on the surface of TiO_2 nanotubes (Li *et al.* 2011). The S_{BET}, crystalline phases, crystallinity, and E_g of TiO_2 nanotubes are also crucial factors that affect the photocatalytic activity. The highest photocatalytic activity was achieved in the presence of the Fe^{3+}-doped catalyst that was calcined at 550 °C, which removed 70.7% of the toluene.

The ionic radius of Ag^+ was significantly larger than that of Ti^{4+} (60.5 pm). The electrons continuously transferred from TiO_2 to Ag_2O on the surface of the TiO_2, which allows the pollutant with negative charges to be easily adsorbed by the catalysts. The f_A of Ag^+ was larger than that of the undoped TiO_2, and the E_g of the catalyst was narrower. The anatase phase exhibited a higher activity (Pang & Abdullah 2012a). The reactor was not protected from light during the experiments. Thus, the visible light in the laboratory promoted the degradation of toluene in the presence of ion-doped TiO_2. Therefore, the catalytic activity of Ag^+-doped TiO_2 increased.

The photocatalytic activity increased when TiO_2 was doped by Al^{3+} or Fe^{3+} ions. The ionic radii of Al^{3+} (53.5 pm) and Fe^{3+} (55 pm) are smaller than that of Ti^{4+}; thus, the ions are easily substituted in the lattice. Two doped ions replace two Ti^{4+} ions, and one O^{2-} hole appears. The shape of the crystal changes, which facilitates the generation of the electron-hole pairs. The f_A increased after ion-doping, and the E_g was narrower.

Doping TiO_2 with V^{5+}, whose valence is higher than that of the parent Ti^{4+}, results in an increase in the concentration of electrons in the conduction band. An upward shift of the Fermi energy level is also expected. When the dopant concentration increases, the surface barrier becomes higher, and the space charge region becomes narrower. The electron-hole pairs within this region are efficiently separated by the large electric field traversing the barrier before these pairs have the chance to recombine (Kiriakidou *et al.* 1999).

The ionic radii of Cu^{2+}, Mn^{2+}, Ni^{2+} and Zn^{2+}, which are 73, 67, 69, and 74 pm respectively, are slightly larger than that of Ti^{4+}. The compounding of TiO_2 and doped-metal causes the generation of Ti^{3+}. The electrons are transferred to Ti^{3+} and then to the oxygen, which reduces the probability for recombination between electrons and holes. In addition, the holes left in the valence band have more opportunity to participate in the oxidizing reactions because the electrons are effectively scavenged by the doping-ions (Zang *et al.* 1995).

Influence of calcination temperature

Fe^{3+}-doped TiO_2 nanotubes containing 1.0% of Fe^{3+} calcined at 450, 500, 550 and 600 °C were prepared to investigate the effect of the calcination temperature. The E_g of the abovementioned catalysts were 3.16, 3.12, 3.06,

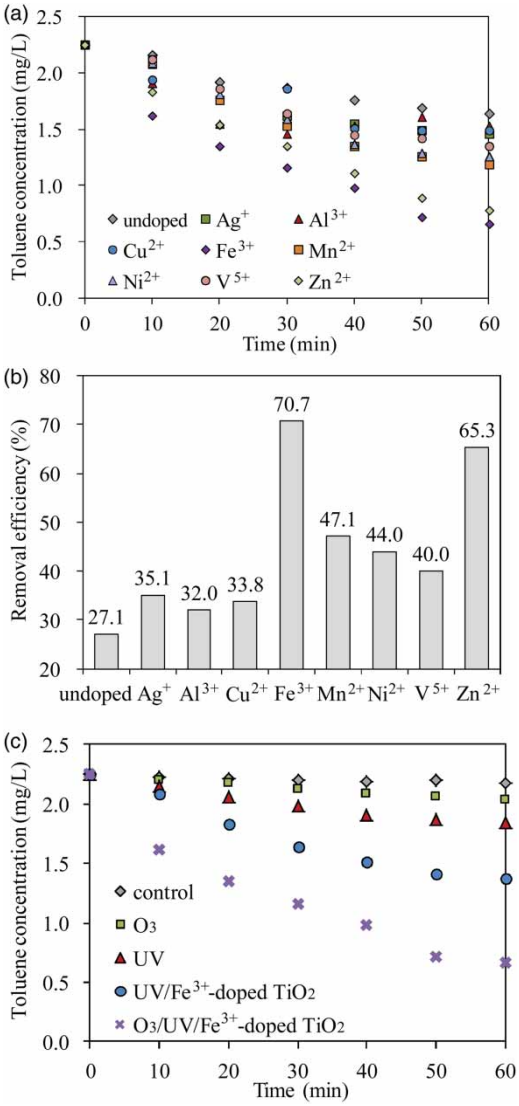

Figure 2 | Removal of toluene for different TiO_2 nanotubes under 254 nm UV irradiation for 60 min. (a) Degradation of 2.25 mg/L toluene versus irradiation time; (b) removal efficiency of toluene for different catalysts; (c) degradation of toluene by O_3, UV, UV/Fe^{3+}-doped TiO_2 and O_3/UV/ Fe^{3+}-doped TiO_2 processes.

and 2.75 eV, whereas the S_{BET} were 122, 120, 118, and 111 m^2/g, respectively. The toluene removal efficiencies for the abovementioned catalysts were 40.1%, 62.3, 70.7, and 35.6%, respectively. When the calcination temperature increases, the E_g and S_{BET} decrease; the f_A increases at first, and then decreases. The E_g was broadened although the S_{BET} of TiO_2 nanotubes calcined at 450 and 500 °C are larger. This result lowered the photocatalytic activity. For the 600 °C calcined catalyst, the f_A and S_{BET} decreased; thus, the overall efficiency is low. TiO_2 nanotubes calcined at 550 °C had preferred crystallinity, S_{BET}, and E_g, which resulted in a higher catalytic activity.

Influence of doping concentration

Fe^{3+}-doped TiO_2 nanotubes with Fe^{3+} doping concentration of 0.1, 0.5, 1.0, and 5.0% calcined at 550 °C were prepared. The f_A of the abovementioned catalysts were 89.1, 90.3, 87.5, and 87.3%, whereas the E_g were 3.10, 3.08, 3.06, and 3.05 eV, and S_{BET} were 170, 141, 118, and 89 m^2/g, respectively. The toluene removal efficiencies for the abovementioned catalysts were 47.8, 61.1, 70.7, and 27.3%, respectively. The f_A of Fe^{3+}-doped TiO_2 increases at first, and then decreases because when TiO_2 is doped by Fe^{3+} ions, the formation of anatase from the amorphous phase is promoted. However, rutile phase formation is significantly promoted when the Fe^{3+} doping concentrations increased. The decline in the phase-transformation temperature can be explained in two ways. First, is that the surface defect density of the TiO_2 nanotubes increases when TiO_2 is doped with Fe^{3+}. These defects act as rutile nucleation sites. Second, is that the surface oxygen vacancy concentration of the anatase grains increases in the ion-doped TiO_2 nanotubes and favors the rearrangement of ions as well as the reorganization of the structure to form the rutile phase (Li *et al.* 2011). The highest photocatalytic activity was achieved in the presence of 1.0% Fe^{3+}-doped TiO_2 under the effects of all the aforementioned factors.

Mechanism of O_3/UV/Fe^{3+}-doped TiO_2 progress

The efficiencies of O_3, UV, UV/Fe^{3+}-doped TiO_2 and O_3/UV/ Fe^{3+}-doped TiO_2 processes for toluene decomposition were also determined. The removal efficiencies for the abovementioned processes were 9.3%, 17.8%, 38.7% and 70.7%, respectively, whereas 3.1% of the toluene volatilized (Figure 2(c)). Compared with other processes, ozonation has a lower toluene decomposition rate because of the lower oxidizability of O_3 compared with that of the •OH generated by the AOP process. The removal efficiency of the UV/Fe^{3+}-doped TiO_2 process was lower than that of the O_3/UV/Fe^{3+}-doped TiO_2 process, indicating that toluene removal in the UV/Fe^{3+}-doped TiO_2 process can be enhanced by ozonation (Yuan *et al.* 2013).

UV and Fe^{3+}-doped TiO_2 can enhance the production of •OH through ozonation progress (Equations (4) and (5)) (Wei *et al.* 2011). A valence band electron could be promoted to the conduction band, thereby leaving holes at the valence band (Equation (6)). Fe^{3+} in TiO_2 acts as

a shallow trapping site for charge carriers shown in Equations (7) and (8) (Pang & Abdullah 2012b). The unstable Fe^{2+} and Fe^{4+} react with H_2O_2 and OH^-, and they transfer to Fe^{3+} as shown in reactions (9) and (10) (Wei *et al.* 2011).

$$O_3 + H_2O + h\gamma \rightarrow O_2 + H_2O_2 \quad (4)$$

$$2O_3 + H_2O_2 \rightarrow 2{}^{\bullet}OH + 3O_2 \quad (5)$$

$$TiO_2 + h\gamma \rightarrow TiO_2(e^- + h^+) \quad (6)$$

$$Fe^{3+} + e^- \rightarrow Fe^{2+} \quad (7)$$

$$Fe^{3+} + h^+ \rightarrow Fe^{4+} \quad (8)$$

$$Fe^{2+} + H_2O_2 \rightarrow Fe^{3+} + {}^{\bullet}OH + OH^- \quad (9)$$

$$Fe^{4+} + OH^- \rightarrow Fe^{3+} + {}^{\bullet}OH \quad (10)$$

$$Fe^{2+} + H_2O_2 \rightarrow Fe(OH)^{2+} + {}^{\bullet}OH \quad (11)$$

$$Fe(OH)^{2+} + h\gamma \rightarrow Fe^{2+} + {}^{\bullet}OH \quad (12)$$

The generated $^{\bullet}OH$ is a powerful oxidizing agent that can attack toluene. Therefore, toluene was efficaciously removed from the water.

CONCLUSIONS

Ion-doped TiO_2 nanotubes were prepared using Degussa P-25 TiO_2 powders. The ions were effectively incorporated into the TiO_2 lattice, except for Ag^+. When TiO_2 is doped by ions, the S_{BET} decreases, and the E_g becomes narrower. The photocatalytic activities of catalysts increased when Ag^+, Al^{3+}, Cu^{2+}, Fe^{3+}, Mn^{2+}, Ni^{2+}, V^{5+}, and Zn^{2+} were doped into the TiO_2 nanotubes. Moreover, the 1.0% Fe^{3+}-doped TiO_2 nanotubes calcined at 550 °C had the highest catalytic activity because of the effects of the f_A, S_{BET}, E_g, and ion-doping. The toluene removal in the UV/Fe^{3+}-doped TiO_2 process can be enhanced by ozonation. The mechanism of O_3/UV/Fe^{3+}-doped TiO_2 progress was that the generated $^{\bullet}OH$ could attack toluene at the surface of TiO_2 or near it.

ACKNOWLEDGEMENT

We gratefully acknowledge the financial support from the National Natural Science Foundation of China (51178043).

REFERENCES

Adewuyi, Y. G. 2001 Sonochemistry: environmental science and engineering applications. *Ind. Eng. Chem. Res.* **40** (22), 4681–4715.

Carp, O., Huisman, C. L. & Reller, A. 2004 Photoinduced reactivity of titanium dioxide. *Prog. Solid State Ch.* **32** (1–2), 33–177.

Epifani, M., Giannini, C., Tapfer, L. & Vasanelli, L. 2000 Sol-gel synthesis and characterization of Ag and Au nanoparticles in SiO_2, TiO_2, and ZrO_2 thin films. *J. Am. Ceram. Soc.* **83** (10), 2385–2393.

Kiriakidou, F., Kondarides, D. I. & Verykios, X. E. 1999 The effect of operational parameters and TiO_2-doping on the photocatalytic degradation of azo-dyes. *Catalysis Today* **54** (1), 119–130.

Leinen, D., Lassaletta, G., Fernandez, A., Caballero, A., Gonzalez-Elipe, A. R., Martin, J. M. & Vacher, B. 1996 Ion beam induced chemical vapor deposition procedure for the preparation of oxide thin films. II. Preparation and characterization of $Al_xTi_yO_z$ thin films. *J. Vacuum Sci. Technol. A* **14** (5), 2842–2848.

Li, X., Zou, X., Qu, Z., Zhao, Q. & Wang, L. 2011 Photocatalytic degradation of gaseous toluene over Ag-doping TiO_2 nanotube powder prepared by anodization coupled with impregnation method. *Chemosphere* **83** (5), 674–679.

Lin, C. & Lin, K. S. 2007 Photocatalytic oxidation of toxic organohalides with TiO_2/UV: The effects of humic substances and organic mixtures. *Chemosphere* **66** (10), 1872–1877.

Pang, Y. L. & Abdullah, A. Z. 2012a Comparative study on the process behavior and reaction kinetics in sonocatalytic degradation of organic dyes by powder and nanotubes TiO_2. *Ultrason. Sonochem.* **19** (3), 642–651.

Pang, Y. L. & Abdullah, A. Z. 2012b Effect of low Fe^{3+} doping on characteristics, sonocatalytic activity and reusability of TiO_2 nanotubes catalysts for removal of Rhodamine B from water. *J. Hazard. Mater.* **235–236**, 326–335.

Ravichandran, L., Selvam, K., Krishnakumar, B. & Swaminathan, M. 2009 Photovalorisation of pentafluorobenzoic acid with platinum doped TiO_2. *J. Hazard. Mater.* **167** (1–3), 763–769.

Spurr, R. A. & Myers, H. 1957 Quantitative analysis of anatase-rutile mixtures with an X-ray diffractometer. *Analyt. Chem.* **29** (5), 760–762.

Sun, L., Li, J., Wang, C. L., Li, S. F., Chen, H. B. & Lin, C. J. 2009 An electrochemical strategy of doping Fe^{3+} into TiO_2 nanotube array films for enhancement in photocatalytic activity. *Sol. Energy Mater. Sol. Cells* **93** (10), 1875–1880.

Takeuchi, M., Hidaka, M. & Anpo, M. 2012 Efficient removal of toluene and benzene in gas phase by the TiO_2/Y-zeolite hybrid photocatalyst. *J. Hazard. Mater.* **237–238**, 133–139.

Wang, W., Varghese, O. K., Paulose, M. & Grimes, C. A. 2004 A study on the growth and structure of titania nanotubes. *J. Mater. Res.* **9** (2), 417–422.

Wei, M. C., Wang, K. S., Hsiao, T. E., Lin, I. C., Wu, H. J., Wu, Y. L., Liu, P. H. & Chang, S. H. 2011 Effects of UV irradiation on humic acid removal by ozonation, Fenton and Fe_0/air treatment: THMFP and biotoxicity evaluation. *J. Hazard. Mater.* **195**, 324–331.

Yu, J., Xiang, Q. & Zhou, M. 2009 Preparation, characterization and visible-light-driven photocatalytic activity of Fe-doped titania nanorods and first-principles study for electronic structures. *Appl. Catal. B: Environ.* **90** (3–4), 595–602.

Yuan, R., Zhou, B., Hua, D. & Shi, C. 2013 Enhanced photocatalytic degradation of humic acids using Al and Fe co-doped TiO_2 nanotubes under UV/ozonation for drinking water purification. *J. Hazard. Mater.* **262**, 527–538.

Zang, L., Liu, C. Y. & Ren, X. M. 1995 Photochemistry of semiconductor particles: Part 4. – Effects of surface condition on the photodegradation of 2,4-dichlorophenol catalysed by TiO_2 suspensions. *J. Chem. Soc. Faraday Trans.* **91** (5), 917–923.

Zhang, G. W., He, G. H., Xue, W. L., Xu, X. F., Liu, D. N. & Xu, Y. H. 2012 Enhanced photocatalytic performance of titania nanotubes modified with sulfuric acid. *J. Mole. Catal. A: Chem.* **363–364**, 423–429.

Zwilling, V., Darque-Ceretti, E., Boutry-Forveille, A., David, D., Perrin, M. Y. & Aucouturier, M. 1999 Structure and physicochemistry of anodic oxide films on titanium and TA6 V alloy. *Surf. Interface Analysis* **27** (7), 629–637.

First received 30 September 2013; accepted in revised form 28 January 2014. Available online 13 February 2014